POLITECNICO
MILANO 1863

SCUOLA DI INGEGNERIA INDUSTRIALE
E DELL'INFORMAZIONE

Executive Summary of the Thesis

Modelling Strategies for Non-Invasive Assessment of Coronary Fractional Flow Reserve

Laurea Magistrale in Biomedical Engineering - Ingegneria Biomedica

Author: Giulia Frigerio

Advisor: Prof. Alberto Redaelli, PhD

Co-advisor: Guido Nannini, MSc

Academic year: 2021-2022

1. Introduction

Cardiovascular diseases (CVDs) are the leading cause of death worldwide. Coronary artery disease (CAD) accounts for 32.7% of CVDs. Coronary arteries supply blood to the myocardium, thus an adequate flow-rate is crucial to maintain the integrity of the cardiac muscle. CAD is usually due to the build-up of plaques that narrow the vascular lumen (i.e., atherosclerosis), and possible consequences can include myocardial infarction and sudden cardiac death. Invasive coronary angiography (ICA) with fractional flow reserve (FFR) evaluation is considered the gold standard for assessing the hemodynamic significance of coronary stenosis. FFR is calculated during maximum hyperemia as the averaged ratio of distal to proximal pressure. If the FFR is <0.80 revascularization is required. In recent years, combining computed tomography coronary angiography (CCTA) and computational fluid dynamic techniques has emerged as a new non-invasive and reliable technique to replace ICA, through which it is possible to non-invasively assess FFR. CCTA derived FFR (FFR_{CT}) has shown high diagnostic accuracy when compared to invasive FFR (iFFR). Research has been pushed towards innovative computational approaches to evaluate FFR_{CT}. The aim of this thesis work was to test different approaches for coronary flow CFD simulations and study the feasibility and accuracy of using simpler yet efficient models in the calculation of FFR_{CT}.

2. Related works

FFR_{CT} analysis requires the following steps: *i*) 3D reconstruction of patient-specific coronary geometry from CT images; *ii*) Assignment of accurate boundary conditions (BCs); *iii*) Numerical solution of the incompressible Navier-Stokes equations (NSEs); *iv*) Post-processing. The pioneer research group was Taylor and colleagues' [4], which investigated both an idealized and a patient-specific geometry in steady-state and transient condition, coupled to lumped parameter models (LPMs) of the downstream microcirculation. Later, Lo et al. [1] explored the use of a simpler LPM as outlet BC (i.e., a 2-elements Windkessel) and analysed the feasibility of using a steady-state simulation instead of a transient one, obtaining a good agreement with iFFR. In general, the results obtained with FFR_{CT} and iFFR have shown an high correspondence between the two diagnostic tools.

The obstacles to the widespread adoption of this innovative approach in clinical diagnostics are twofold. Firstly, clinicians are not familiar with computational techniques used in patient-specific CFD models, leading to reluctance to embrace this approach. Secondly, the approach is time-consuming, which adds to its lack of popularity. Recent works [1] have supported the idea that even simpler models could led to accurate FFR_{CT} results. This significant conclusion marks a crucial initial stride towards incorporating this methodology as a diagnostic tool in clinical practice.

3. Material and Methods

Incrementally more complex scenarios with different degrees of stenosis were simulated and analysed. Firstly, idealized stenosis geometries coupled to BCs based on average population pressure and flow data were simulated; then patient-specific geometries reconstructed from CCTA, coupled with average population-based BCs and finally with patient-specific BCs, were simulated. Since diagnostic indexes as FFR are based on average values over the cardiac cycle, with the aim of reducing the computational time, the possibility of using a steady-state simulation rather than a transient one was investigated. To validate the developed model, the computed FFR_{CT} was compared against iFFR.

3.1. Idealized Geometry

The idealized geometry consisted in a pipe with different degrees of stenosis, ranging from 50 to 80%. The geometry was meshed using tetrahedral elements with an element size of 0.25 mm and a body sizing reduction of of 0.125 mm in the stenosis region. Blood flow and pressure fields were obtained solving NSEs. Blood was modelled as a Newtonian fluid with a constant viscosity $\mu = 0.003\ Pa \cdot s$ and density $\rho = 1060\ kg/m^3$. At the wall boundaries, a no-slip condition was enforced. As inlet BC a pressure waveform was applied. Trying to replicate the ideal model described in Ref.[4], pressure was set to 90 mmHg. For transient simulations, a literature pressure waveform with a mean pressure of 90 mmHg was applied.
At the outlet surface, a LPM consisting of a resistance element was imposed in the steady-state simulations, while in the transient one

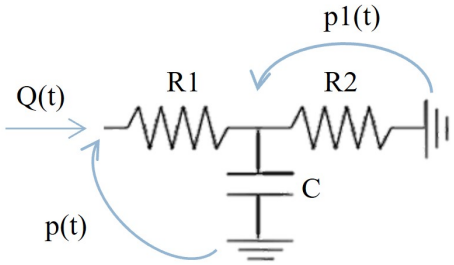

Figure 1: 3WK imposed as outlet BC.

	Coronary Artery	**iFFR**
Patient-1	LAD	0.76
Patient-6	RCA	0.57
Patient-9	RCA	0.94
Patient-10	LAD	0.83

Table 1: Selected patients to validate the proposed model, with relative iFFR value.LAD: Left dominant coronary artery, RCA: right coronary artery.

a 3-elements Windkessel (WK3) was applied (**Figure 1**). The total resistance was set equal to the resistance value used in the steady simulation, then it was split between proximal (R1) and distal (R2) resistance based on a 3:7 ratio. Compliance (C) value was based on literature values [5]. The R1, R2 and C values were finally tuned by minimizing the error between the resulting flow obtained for the prescribed inlet pressure wave and a physiological flow-rate waveform of the left coronary artery (LCA). Transient simulation was run for 5 cardiac cycles with a time-step equal to 0.001 s. Solution was considered converged when residuals were below 10^{-5}. Results were then post-processed to extract FFR_{CT}.

3.2. Patient-specific Geometry

Among a dataset consisting of 10 CCTA, four subjects were retrieved, based on the measured iFFR in order to have a dataset sufficiently representative of the stenosis severity (**Table 1**). The adopted workflow to estimate FFR_{CT} value from patient-specific coronary artery geometries is shown in **Figure 2**.

CT image segmentation and 3D anatomy reconstruction. The segmentation of LCA, RCA and calcific plaque was manually per-

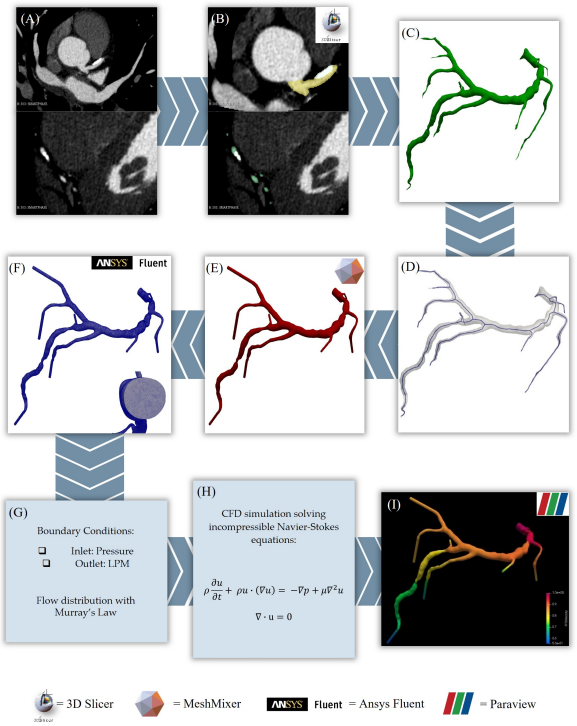

Figure 2: Workflow adopted to estimate the FFR_{CT}. (**A**) CCTA images. (**B**) Segmentation of LCA (in yellow), RCA (in green) and plaque (in white). (**C**) 3D model reconstruction. (**D**) Centreline extraction. (**E**) Refined geometry. (**F**) Meshed geometry. (**G**) Imposition of appropriate boundary conditions. (**H**) CFD simulations and (**I**) analysis of the obtained results.

formed on CT images acquired at Centro Cardiologico Monzino (Milano, Italy) in open-source software 3DSlicer. After having obtained a rough reconstruction of the patient geometry, refinements were performed to prepare the geometry for the CFD simulation.

Meshing. Mesh sensitivity analysis was conducted to define the most appropriate element size (ES). Specifically a coarse (ES=0.25 mm), medium (ES=0.1 mm) and fine (ES=0.07 mm) mesh were tested by simulating a steady flow. The ratio between upstream and downstream pressure to the stenosis was used as grid convergence index (GCI).

Material Properties Flow was assumed to be laminar and incompressible, while the blood was assumed to behave as a Newtonian fluid. Blood density and viscosity were set to 1060 kg/m^3 and 0.0035 Pa $\cdot$ s, respectively.

Boundary Conditions

BCs based on Average Literature Values The aim of the first set of simulations was to compare the results obtained through a steady-state and a transient simulation. At the inlet surface a pressure waveform ranging from 80 to 120 mmHg, was set in all the patients. For the steady simulation, the average value was imposed. A 3WK was applied as BC at the outlet surfaces. In this model, venous pressure was set to 0 mmHg, and the intramyocardial pressure was not accounted for. To determine resistance values, the first step is the estimation of total coronary flow. Flow rate in coronary arteries is approximately 4% of CO thus considering a CO of 6 lpm, the adopted resting coronary flow was 250 ml/min. It was then subdivided in LCA and RCA with a 6:4 proportion. Flow distribution in each coronary branch was performed accordingly to Murray's Law. In order to reproduce the max hyperaemic condition resting coronary flow was increased by 4-folds. Each coronary outlet resistance can be then calculated as follow:

$$R_i^{hyp} = \frac{MAP - P_v}{Qout_i^{hyp}} \tag{1}$$

R_i^{hyp} was then subdivided in R1 and R2 with a 3:7 ratio. Total compliance value for either LCA and RCA was taken from the literature and then subdivided in the coronary branches proportionally to their cross-sectional area. R1, R2 and C were then tuned to obtain a flow-rate waveform with an average value approximately equal to the flow calculated with Murray's Law. For the steady simulation a total resistance was calculated by the sum of the optimal R1 and R2.

BCs based on Patient-Specific Data The available patient-specific data were: gender, age, weight, height, minimum and maximum aortic pressure, heart rate (HR) at rest and under hyperaemic condition. For steady simulations, mean aortic pressure (MAP) was calculated as a function of HR, systolic blood pressure (SBP) and diastolic blood pressure (DBP) [3]. For the transient simulations instead, the pressure wave adopted in the simulation with the first set of BCs was scaled in order to match the SBP and DBP of each patient. Patient-specific CO was estimated from a stroke volume (SV) [2] given by:

$$SV = PP^* \cdot [(0.013 \cdot W) - (0.007 \cdot Y) + - (0.004 \cdot HR_{rest}) + 1.307] \quad (2)$$

where W is the weight in kilograms, Y the age and HR_{rest} the resting heart rate. PP* is calculated as follows:

$$PP^* = (0.49 \cdot PP) + (0.3 \cdot Y) + 7.11 \quad (3)$$

where PP is the pulse pressure calculated as BSP-BDP in which BSP and BDP are in mmHg. Firstly, coronary flow was distributed between LCA and RCA using a 6:4 proportion. Later, coronary hyperaemic flow needed to be imposed. Total coronary resistance index (TCRI) was calculated based on patient's hyperaemic HR [3]. Coronary hyperaemic flow-rate was then derived by dividing the resting value by the patient-specific TCRI. It was split between branches as described in the previous Section and finally 3WK parameters were optimized using the same procedure adopted for the 1st set of BCs.

CFD Simulations. CFD simulations were run in ANSYS Fluent. The simulations were run using a SIMPLE method with a 2nd order computational scheme. Transient simulations were run for 5 cardiac cycle using a time-step of 0.001 s. For all the simulation a convergence criteria of 10^{-5} was adopted. After each simulation was terminated, the resulting inlet flow-rate was compared to the expected one (based on the imposed BCs). An in-house code was implemented to tune the LPM in such a way that a difference between expected and resulting flow-rate was $\leq 10\%$.

Post-Processing. The obtained pressure and velocity fields were imported in Paraview for the post-processing, to extract FFR_{CT}. It was then examined if there was agreement between FFR_{CT} and iFFR in terms of clinical indication, whether to revascularise or not, based on a cut-off threshold of 0.80. The agreement is equal to 1 if both ≤ 0.80 or > 0.80, 0 otherwise.

4. Results

4.1. Idealized Geometry

A map of FFR for pipes with degrees of stenosis ranging from 50% to 80% is presented in **Figure 4** for both steady-state and transient simulations. For increasing degrees of stenosis Steady FFR (FFR_{SS}) becomes significantly lower if compared to Transient FFR (FFR_T). This means a greater pressure drop is present in the steady-state simulations. To further investigate this difference, vorticity was derived from the extracted velocity field. Its maximum values were found in each case at the throat section of the stenosis. As the obstruction level increases, the difference between the vorticity obtained in the steady and transient simulations increases as well. Specifically, the vorticity values in the steady-state simulations are notably higher.

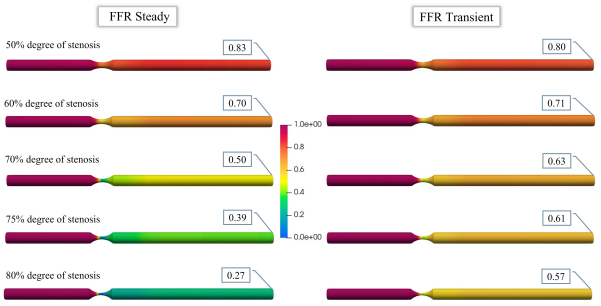

Figure 4: Comparison between FFR_{SS} and FFR_T for progressively increasing degrees of stenosis.

4.2. Patient-specific Geometry

Sensitivity Analysis The values obtained for the GCI were $f_1 = 0.886$, $f_2 = 0.869$ and $f_3 = 0.862$ for the coarse, medium and fine mesh, respectively. As the difference between GCI obtained with medium and fine mesh was $\leq 1\%$, the medium mesh (~ 15 million tetrahedral elements), was selected.

Patient-specific Geometry with BCs based on Averaged Literature Data The divergence between FFR_{SS} and FFR_T was found to be less than 1% in all the four analysed geometries (**Table 2**). The current findings contradict the results obtained from simulations of the idealized geometry. No significant differences were observed, even for more severe degrees of stenosis (i.e.. Patient-6)(**Figure 3**). Also in this case though, vorticity was derived from the velocity field. Contrary to what happened in the idealized geometry, no particular difference in vorticity was found (max difference $\sim 6\%$).

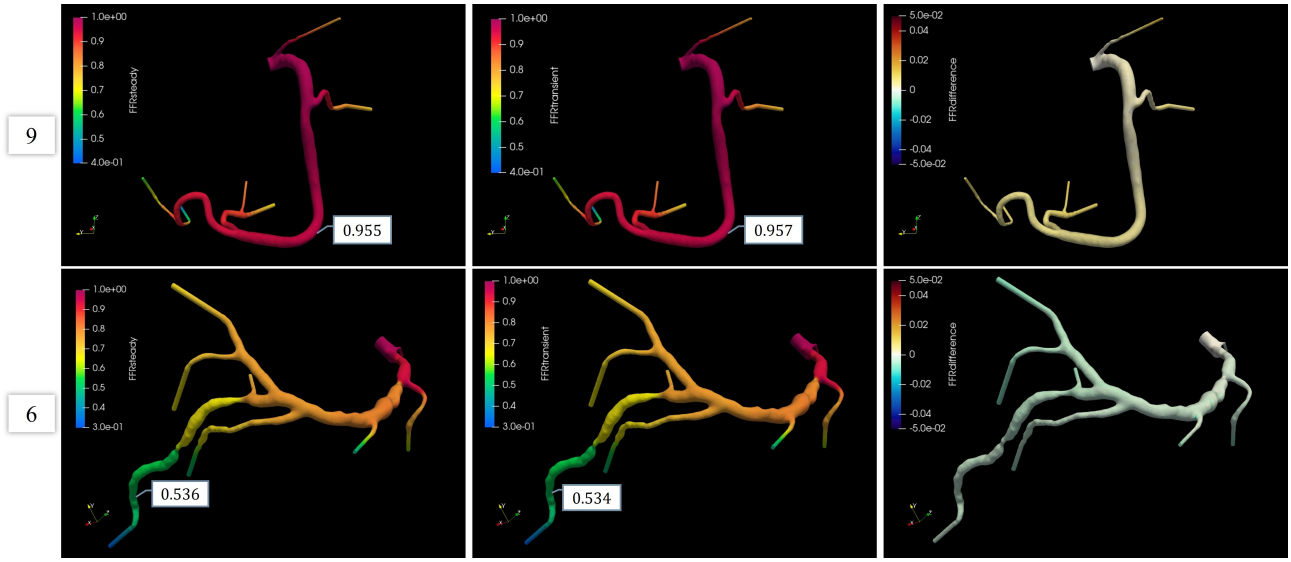

Figure 3: Comparison between FFR_{SS} and FFR_T for patients with the lower (Patient-9) and higher (Patient-6) degrees of stenosis.

Patient	FFR_{SS}	FFR_T	ϵ_r
1	0.884	0.892	0.89%
6	0.536	0.534	0.37%
9	0.955	0.957	0.21%
10	0.932	0.940	0.85%

Table 2: Comparison between FFR_{SS} and FFR_T obtained from the set of simulations with BCs based on average literature data.

Patient	ϵ_{SS}	ϵ_T	Agreement
1	19.73%	20.39%	0
6	6.10%	4.56%	1
9	1.38%	2.12%	1
10	10.24%	10.84%	1

Table 3: Relative error between FFR_{SS} and FFR_T with respect to iFFR.

Patient-specific Geometry with BCs based on Patient-Specific Data The main focus with these simulations was the validation of the method: both FFR_{SS} and FFR_T were compared against iFFR (**Table 3**). A good agreement was found for Patient-6 and -9 ($\epsilon_r \leq 6.5\%$). A more significant difference is present for Patient-1 and -6. Considering the agreement based on the standard revascularization threshold of 0.80, the FFR of three over four patients is in agreement with the iFFR.

5. Discussion

The initial analysis was conducted on the idealized geometry. The obtained results showed that both FFR_{SS} and FFR_T decrease as the percentage of stenosis increases. The increase in pressure drop can be explained by the higher resistance to flow caused by vessel narrowing, resulting in both distributed losses along the length of the pipe and concentrated losses in the narrowing region. Analysing in more detail, it can be seen that for 50-60% degree of stenosis the $FFR_{SS} \sim FFR_T$, while for more severe narrowing ($> 70\%$), FFR_{SS} tends to overestimate the severity of the stenosis if compared to FFR_T. To better understand this phenomenon, vorticity was examined. As the obstruction level increased, the difference between the maximum vorticity observed with the two simulations approaches also increased, suggesting the formation of longer-lasting swirling structures in the steady case (in which highest vorticity was found). The reason for such results can be attributed to the fact that higher vorticity indicates increased shear stress in boundary regions, leading to greater resistance to flow and in turn, an higher pressure drop.
To isolate the effect of the geometry, FFR_{CT} was then evaluated in patient-specific geometries with BCs based on average literature data. The

obtained results indicate that, in constrast to the idealized geometry, there is no significant difference between FFR_{SS} and FFR_T. The relative error was found to be less than 1% indicating that the hemodynamic distribution computed by FFR_{SS} is essentially identical to that of FFR_T. Similar results were obtained by [1]. These findings suggests that the FFR_{CT} can be accurately estimated with simpler and less time-expensive steady-state simulations. Furthermore, vorticity was also analysed but no significant difference were found. Vorticity resulted higher in idealized simulations with respect to patient-specific ones. This could be attributed to the fact that this geometry had a smaller diameter at the stenosis centre, resulting in higher shear stress and therefore higher vorticity.
Finally, the proposed approach with BCs based on patient-specific data, was validated in relation to iFFR. When examining the results in terms of FFR_{CT}, the outcomes from steady-state and transient simulations were comparable. The proposed approach demonstrated relatively robust performance for Patient-6 and -9, whose RCA was analysed ($\epsilon_r \leq 6.5\%$). However, Patient-1 and -10, whose stenotic vessel was in the LAD, exhibited greater errors. The relatively higher error may have various potential explanations to be considered: *i*) Further investigations are necessary to obtain more reliable patient-specific coronary flow-rates; *ii*) A 3WK was imposed as outlet BC, but some aspects that are not included in this model may be crucial. Intramyocardial pressure, for example, has shown to have an higher influence in the LCA if compared to RCA. Thus it may be necessary to account for it in LCA branches; *iii*) Errors may have been introduced during the segmentation process; *iv*) Considering the stenosis geometry, no sudden decrease in diameter is present and furthermore, the minimum lumen diameter has demonstrated to have the highest impact on FFR_{CT} uncertainty, with a greater effect in the LAD. While these are some possible explanations for the obtained discrepancies, further investigations should be conducted.
*Limitations and Future Developments.*The developed CFD model is subject to certain limitations and approximations, which serve as a foundation for future developments. The main aspects that need to be improved are: patient pool, coronary flow-rate, BCs, patient-specific hyperemic condition, iFFR location, computational cost.

6. Conclusions

The proposed CFD model has demonstrated promising results in non-invasively estimating FFR_{CT}. In efforts to decrease the computational time, accordingly to the results obtained, adopting steady-state simulations over transient ones is recommended. Both patients with mild to severe degrees of stenosis have been included in this work. A strong agreement was observed when comparing FFR_{CT} values with iFFR for patients with measurement performed in the RCA, but further investigations are necessary for patients who had a stenosis in the LAD. While the preliminary results are positive, the impact of different parameters (i.e. TCRI, intramyocardial pressure, patient-specific coronary flow-rate ...) requires further exploration. Future research should be conducted with a wider range of patients.

References

[1] E. WC Lo, L. J Menezes, and R. Torii. Impact of inflow boundary conditions on the calculation of ct-based ffr. *Fluids*, 4(2):60, 2019.

[2] L. O Müller, F. E Fossan, A. T Bråten, A. Jørgensen, R. Wiseth, and L. R Hellevik. Impact of baseline coronary flow and its distribution on fractional flow reserve prediction. *Int J Numer Methods Eng*, 37(11):e3246, 2021.

[3] P. Sharma, L. Itu, X. Zheng, A. Kamen, D. Bernhardt, C. Suciu, and D. Comaniciu. A framework for personalization of coronary flow computations during rest and hyperemia. pages 6665–6668, 2012.

[4] C.A. Taylor, T. A. Fonte, and J. K. Min. Computational fluid dynamics applied to cardiac computed tomography for noninvasive quantification of fractional flow reserve: Scientific basis. *JACC*, 61:2233–2241, 6 2013.

[5] M. Yin, A. Yazdani, and G. E. Karniadakis. One-dimensional modeling of fractional flow reserve in coronary artery disease: Uncertainty quantification and bayesian optimization. *Comput Methods Appl Mech Eng*, 353:66–85, 2019.